Somatic uniparental disomy mitigates the most damaging *EFL1* allele combination in Shwachman-Diamond syndrome

Sangmoon Lee[1,*,15], Chang Hoon Shin[2,*,15], Jawon Lee[1], Seong Dong Jeong[2], Che Ry Hong[3], Jun-Dae Kim[4], Ah-Ra Kim[5], Soo Jin Son[6,7], Oleksandr Kokhan[8], Taekyeong Yoo[1], Jae Sung Ko[3], Young Bae Sohn[9], Ok-Hwa Kim[10], Jung Min Ko[3], Tae-Joon Cho[11], Nathan T. Wright[8], Je Kyung Seong[6,7,12], Suk-Won Jin[4,5], Hyoung Jin Kang[3,13,**], Hyeon Ho Kim[2,14,**], Murim Choi[1,3,**]

[1]Department of Biomedical Sciences, Seoul National University College of Medicine, Seoul, Republic of Korea.

[2]Department of Health Sciences and Technology, Samsung Advanced Institute for Health Sciences and Technology, Sungkyunkwan University, Seoul, Republic of Korea.

[3]Department of Pediatrics, Seoul National University College of Medicine, Seoul, Republic of Korea.

[4]Yale Cardiovascular Research Center, Section of Cardiovascular Medicine, Department of Internal Medicine, Yale University School of Medicine, New Haven, CT, USA.

[5]School of Life Sciences, Gwangju Institute of Science and Technology, Gwangju, Republic of Korea.

[6]Laboratory of Developmental Biology and Genomics, Research Institute for Veterinary Science, and BK21 PLUS Program for Creative Veterinary Science Research, College of Veterinary Medicine, Seoul National University, Seoul, Republic of Korea.

[7]Korea Mouse Phenotyping Center (KMPC), Seoul National University, Seoul, Republic of Korea.

[8]Department of Chemistry and Biochemistry, James Madison University, Harrisonburg, VA, USA.

[9]Department of Medical Genetics, Ajou University Hospital, Ajou University School of Medicine, Suwon, Republic of Korea.

[10]Department of Pediatric Radiology, VIC 365 Children's Hospital, Incheon, Republic of Korea.

[11]Department of Orthopaedic Surgery, Seoul National University College of Medicine, Seoul, Republic of Korea.

[12]Interdisciplinary Program for Bioinformatics, Program for Cancer Biology and BIO-MAX/N-Bio Institute, Seoul National University, Seoul, Republic of Korea.

[13]Seoul National University Cancer Research Institute, Seoul, Republic of Korea.

[14]Institute for Future Medicine, Samsung Medical Center, Seoul, Republic of Korea

*S. Lee, and C.H. Shin contributed equally to this paper.

** H.J. Kang, H.H.Kim, and M.Choi contributed equally to this paper

Correspondence to Murim Choi: murimchoi@snu.ac.kr; or Hyeon Ho Kim: hyeonhkim@skku.edu or Hyoung Jin Kang: kanghj@snu.ac.kr

[15]Current address: Sangmoon Lee (Department of Neurosciences, University of California, San Diego, La Jolla, CA 92093, USA). Chang Hoon Shin (Laboratory of Genetics and Genomics, National Institute on Aging Intramural Research Program, National Institutes of Health, Baltimore, MD 21224, USA).

Abstract

Shwachman-Diamond syndrome (SDS; OMIM: #260400) is caused by variants in *SBDS* (Shwachman-Bodian-Diamond syndrome gene), which encodes a protein that plays an important role in ribosome assembly. Recent reports suggest that recessive variants in *EFL1* are also responsible for SDS. However, the precise genetic mechanism that leads to *EFL1*-induced SDS remains incompletely understood. Here we present three unrelated Korean SDS patients that carry biallelic pathogenic variants in *EFL1* with biased allele frequencies, resulting from a bone marrow-specific somatic uniparental disomy (UPD) in chromosome 15. The recombination events generated cells that were homozygous for the relatively milder variant, allowing for the evasion of catastrophic physiological consequences. Still, the milder *EFL1* variant was solely able to impair 80S ribosome assembly and induce SDS features in cell line, zebrafish, and mouse models. The loss of *EFL1* resulted in a pronounced inhibition of terminal oligo-pyrimidine element-containing ribosomal protein transcript 80S assembly. Therefore, we propose a more accurate pathogenesis mechanism of EFL1 dysfunction that eventually leads to aberrant translational control and ribosomopathy.

Introduction

Patients clinically diagnosed with Shwachman-Diamond syndrome (SDS; OMIM: #260400) present with a constellation of disorders, such as hematologic manifestations, exocrine pancreatic dysfunction with fatty infiltration, and skeletal dysplasia that results in short stature[1-3]. The hematologic manifestations include neutropenia or, less severely, thrombocytopenia and anemia with a predisposition for myelodysplastic syndrome and acute myeloid leukemia transformations[4,5]. Variants in *SBDS* (Shwachman-Bodian-Diamond syndrome gene), which encodes a protein that plays an important role in ribosome assembly, are mainly responsible for the disease[1,6-8]. Thus, SDS is considered to be a ribosomopathy, which is a collective term that is used to describe a group of congenital disorders caused by problems in ribosome biogenesis, assembly or function[9]. Moreover, ~10% of clinically diagnosed SDS cases do not contain any pathogenic *SBDS* variants, suggesting the existence of additional genetic mechanisms that lead to the disorder[1,6]. Recent reports demonstrate that variants in genes other than *SBDS*, namely *EFL1*, *DNAJC21,* and *SRP54*, are implicated with bone marrow failure syndrome and SDS[10-15]. Homozygous variants of *EFL1* cause an SDS-like syndrome in a recessive manner, which is highlighted by the observation that three of the seven reported kindreds underwent consanguineous marriages[10,11,15]. EFL1 directly interacts with SBDS to release eukaryotic translation initiation factor

6 (eIF6) from the 60S ribosomal subunit for 80S ribosomal assembly[7,16]. Thus, it needs to be further investigated whether there is an additional genetic mechanism that leads to SDS in outbred populations other than through homozygous pathogenic variants in *EFL1*.

As more human genomes with or without clinical significances continue to be sequenced, it has become clear that variants of unknown significances (VUS) pose a substantial obstacle in the interpretation of genotype-phenotype relationships. As many variants are believed to possess the ability to cause alternations at the molecular level but only with sub-clinical levels of severity, numerous scenarios that enable VUS to acquire clinical significances have been postulated. One of these scenarios involves the assessment of somatically acquired uniparental disomy (UPD) in the hematopoietic system; although only a small number of instances have been previously reported. Notable examples include myeloid neoplasia[17,18], immunodeficiency[19], and a single case of sickle cell disease[20].

In this study, we demonstrated a disease-causing mechanism in patients who inherited compound heterozygous variants in *EFL1*. A mosaic UPD caused a loss-of-heterozygosity (LOH) in the *EFL1* locus in the bone marrow and blood, simultaneously homozygosing the less damaging variant and decreasing the representation of the more damaging variant to avoid worse hematologic phenotypes. However, this still led to EFL1 dysfunction in the bone marrow and resulted in SDS features. We further demonstrated

121 that the remaining variant by the UPD was a hypomorph and pathogenic, by
122 investigating the molecular mechanism of the EFL1 dysfunction in cell and
123 animal models. Therefore, searching for a pathogenic variant that was
124 caused by a non-conventional pathway may increase the probability of
125 identifying the genetic cause and improve our understanding of the disease
126 mechanism, and this approach could possibly benefit additional patients
127 with severe hematological abnormalities.
128

Results

Shwachman-Diamond syndrome patients without *SBDS* variants

We recruited three unrelated and non-consanguineous Korean SDS patients without plausible recessive mutations in *SBDS* (Fig. 1a; Table S1; Supplemental Clinical Narratives). Proband I-1 is a 3-year-old boy who had severe intrauterine growth retardation that resulted in a preterm delivery (35+3 weeks) and a birth weight of 1.7 kg. He had thrombocytopenia, neutropenia, and anemia at 2-months of age. A bone marrow examination performed at 6-months of age revealed hypocellularity, reduced megakaryocytes, and an increase in iron storage. He also had pancreatic lipomatosis, along with an exocrine pancreatic insufficiency, and metaphyseal chondrodysplasia (Fig. 1a; Fig. S1). Proband II-1 is a 9-year-old female who had severe intrauterine growth retardation that resulted in a preterm delivery (36 weeks) and a birth weight of 1.6 kg. She had a diffuse fatty infiltration of the pancreas and metaphyseal chondrodysplasia that was accompanied by osteopenia and short stature (Fig. 1a). Her sister was unaffected. Proband III-1 is a 25-year-old male who did not have any perinatal problems except for a low birth weight (40+4 weeks, 2.4 kg). At 2-years-old, he had pancreatic exocrine and endocrine insufficiencies, thrombocytopenia, anemia, intermittent neutropenia, metaphyseal chondrodysplasia, and ichthyosis. Later, he developed osteoporosis, hepatomegaly, and a total fatty change of the pancreas (Fig. 1a).

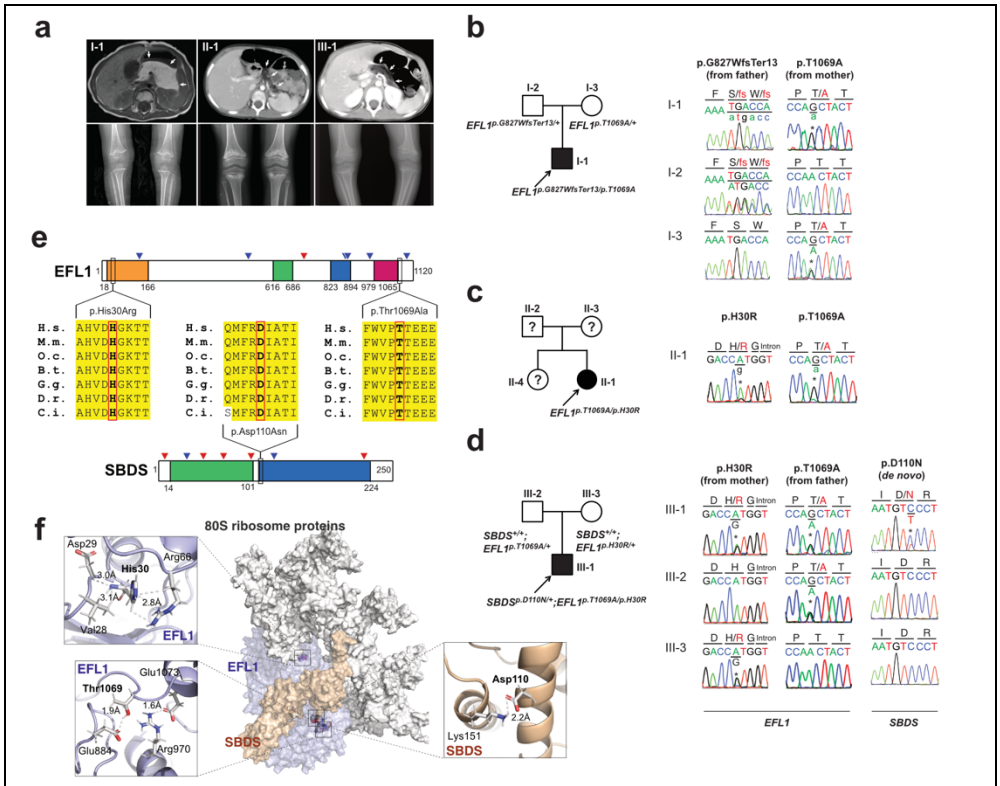

Fig. 1. *EFL1* variants in *SBDS*-negative SDS patients. a Non-contrast T1-weighted abdominal MRI (I-1) or CT images (II-1 and III-1) showing a diffuse enlargement with lipomatosis of the pancreas (arrows) (upper) and both knees with metaphyseal widening and irregularities in the femora in the three patients and associated genu varum in III-1 (lower). **b-d** Pedigrees and Sanger sequencing traces showing the inherited *EFL1* variants and the *de novo* *SBDS*$^{p.Asp110Asn}$ variant in the three families. DNA was extracted from whole blood samples. Note that the lower case nucleotide letters were used on top of the Sanger traces to reflect their minor representation in the patient samples. **e** The residues with nonsynonymous changes in EFL1 and SBDS are evolutionarily conserved. The arrowheads on the protein maps denote previously reported pathogenic variants (Blue: missense, red: LoF). **f** Molecular modeling-based structural analysis using PDB 5ANC[7]. The insets show the detailed interactions involving EFL1 His30, Thr1069 and SBDS Asp110. B.t., *Bos taurus*; C.i., *Ciona*

intestinalis; D.m., *Drosophila melanogaster*; D.r., *Danio rerio*; G.g., *Gallus gallus*; H.s., *Homo sapiens*; M.m., *Mus musculus*; O.c., *Oryctolagus cuniculus*.

152

153 **Identification of mosaic *EFL1* variants**

154 To identify the genetic factors that predisposed the three patients to SDS,
155 we exome-sequenced the patients and the available parental DNA was
156 extracted from whole blood (Table S2). Notably, the heterozygous
157 p.Thr1069Ala variant of *EFL1* (chr15:82,422,872 T>C, hg19,
158 NM_024580.5:c.3205A>G) was identified in all three patients (Fig. 1b-d,
159 Table 1; Table S3), which was not previously found in SDS patients. Based
160 on gnomAD, it is a low frequency variant that was carried by three
161 individuals among 17,972 alleles in the East Asian population (East Asian
162 allele frequency (EA-AF) = 1.7×10^{-4})[21]. Under the assumption that *EFL1*
163 variants function in a recessive manner, we sought to ascertain additional
164 variants that may pose increased damage to the gene function. Remarkably,
165 we found a second variants in *EFL1* in all three patients which were not
166 detected by the initial analysis either due to a low number of variant
167 supporting reads in the proband or due to a low mapping quality caused by
168 the sequence similarity between the *EFL1* and *EFL1P1* loci. Proband I-1
169 carried a paternally-originated frameshift variant p.Gly827TrpfsTer13
170 (chr15:82,444,316 C>CA, hg19, NM_024580.5:c.2478dupT, gnomAD EA-
171 AF = 0) with a minor allele frequency (MAF) of 8.3%, and Proband II-1 and
172 III-1 carried an inherited missense variant p.His30Arg (chr15: 82,554,031
173 T>C, hg19, NM_024580.5:c.89A>G, gnomAD EA-AF = 5.1×10^{-5}) with

174 MAFs of 14.8% and 36.8%, respectively (Table 1). In addition, Proband III-1
175 harbored a heterozygous *SBDS* p.Asn110Asp variant as *de novo* (Fig. 1d;
176 Fig. S2), which is never seen in the control databases. Then we noted that
177 the non-reference allele of *EFL1* p.Thr1069Ala for I-1 and II-1 was
178 dominantly covered compared to the reference allele (Table 1), which
179 caused it to function like an incomplete homozygous variant, while the ratio
180 was comparable in III-1 (Fig. 1c; Table 1). All the *EFL1* variants were equally
181 represented in the parental carriers. The patients did not carry any variant in
182 other SDS-associated genes, including *DNAJC21* and *SRP54* (data not
183 shown). The two EFL1 amino acid residues harboring the missense variants
184 (His30 and Thr1069) are highly conserved throughout evolution and are
185 predicted to be pathogenic (Fig. 1e; Table S4). The protein structure
186 analysis suggested that the His30 and Thr1069 residues form hydrogen
187 bonds with neighboring residues, which would presumably confer stability to
188 the protein structure. Notably, previously reported pathogenic residues
189 Cys883 and Arg970 lie close to Thr1069 (Fig. 1f; Fig. S3)[15]. The SBDS
190 Asn110 reside is also conserved among the vertebrate species (Fig. 1e;
191 Table S4) and is expected to interact with neighboring amino acids,
192 including Lys151 (Fig. 1f).
193 To understand the genetic cause of this observation, we
194 investigated whether large-scale structural variants exist that encompass
195 the region. Indeed, all the patients carried a partial LOH in chromosome 15,
196 where *EFL1* resides (Fig. 2a; Figs. S4 and S5). This LOH was copy-neutral

197 and was not seen in the healthy parents (Fig. S6), suggesting that it was
198 caused by a somatic UPD. This LOH of the *EFL1* locus is not frequently
199 found in healthy Korean individuals (1/3,667 = 2.7 x 10^{-4}, Fig. S7). Also,
200 according to a survey of hematopoietic chromosomal mosaicism events, 117
201 of 151,202 apparently normal individuals carry a copy-neutral LOH or a
202 copy-number deletion of the *EFL1* locus (7.7 x 10^{-4})[22]. Thus, the LOH of the
203 *EFL1* locus is a rare event. The sizes of the LOH intervals were variable
204 among the patients (100%, 100% and 27.8% of the entire chromosome
205 span for I-1, II-1, and III-1, respectively; Fig. 2a). We also sought to identify
206 the haplotype origins of the variants that the probands carried and observed
207 that the chromosomes that were dominantly represented (*i.e.*, the maternal
208 chromosome for I-1 and the paternal chromosome for III-1) harbored
209 *EFL1*$^{p.Thr1069Ala}$, which was consistent with their higher coverage ratios
210 compared to other variants as documented in the WES analysis (Fig. 2a). To
211 test if the UPD event occurred in a mosaic pattern and whether LOH-
212 carrying and non-LOH-carrying cells co-exist, a single-cell SNP microarray
213 experiment was performed using bone marrow (I-1) or cells from buccal
214 swabs (III-1). As expected, complete LOHs in chromosome 15 were
215 observed in a subset of the cells, confirming the mosaic UPD events that
216 preferentially selected *EFL1*$^{p.Thr1069Ala}$ over the other variants (*i.e.*,
217 *EFL1*$^{p.Gly827TrpfsTer13}$ and *EFL1*$^{p.His30Arg}$; Fig. 2b-d; Fig. S8). Therefore, cells
218 containing UPD of chromosome 15 are expected to be homozygous for the
219 *EFL1*$^{p.Thr1069Ala}$ allele and be a homozygous reference for the other two

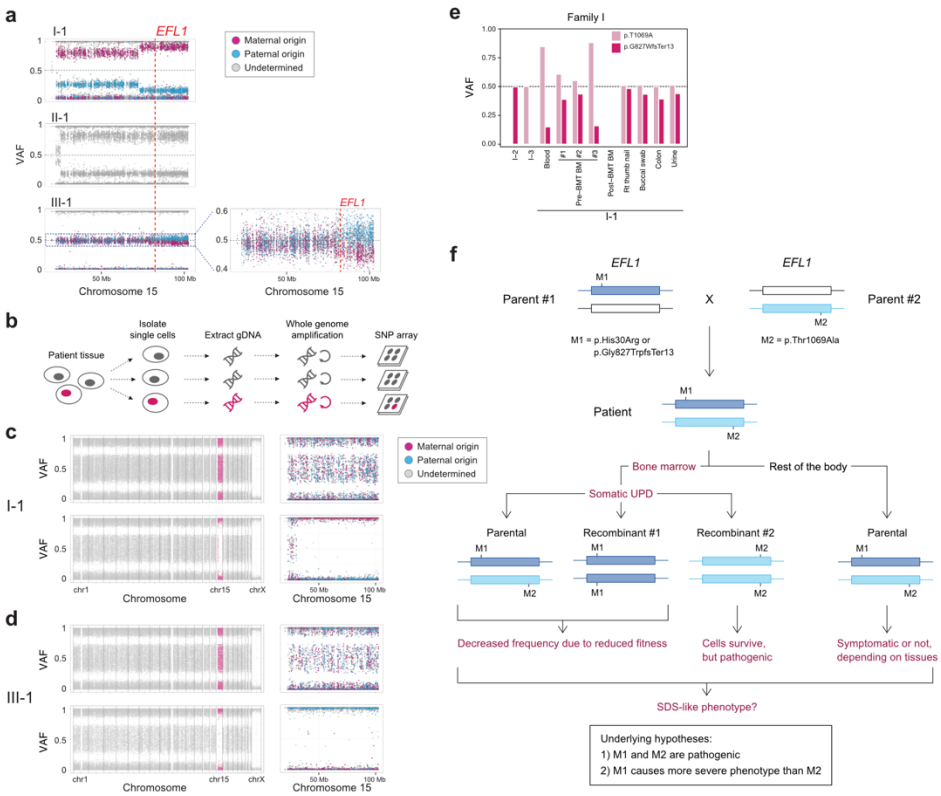

Fig. 2. *EFL1* variants display somatic mosaicism. a All three patients demonstrate a partial LOH in chromosome 15, as indicated by the deviation from VAF 0.5. The variant origin is indicated by the red or blue dots, whereas parental samples were not available for II-1. The location of *EFL1* is indicated by a red dotted line. **b** Schematic diagram of the single cell LOH experiment shown in c-d, where a red cell symbolizes an LOH-carrying cell. **c-d** Single cell LOH profiles from I-1 bone marrow (**c**) and III-1 buccal swab samples (**d**), the upper plots denote cells without LOH, and the lower plots represent cells with a complete LOH in chr15. The plots on the right show chr15 with the variant origin shown in red or blue dots. **e** VAF of the *EFL1* variant in multiple tissue samples from I-1. VAF, variant allele frequency. **f** Genetic process underlying selection of *EFL1*$^{p.Thr1069Ala}$ cells in the patients.

220

alleles. II-1 was not tested, because the sample was unavailable. Next, we checked the spatial extent of the mosaic UPD by subjecting all available tissue samples from I-1 to a high-depth amplicon sequencing analysis (>10,000X coverage depths). Variant AFs of p.Thr1069Ala in I-1 were ~0.85 in the peripheral blood and bone marrow but ~0.5 in most tissues. Conversely, AFs of p.Gly827TrpfsTer13 in the peripheral blood and bone marrow were ~0.15 and displayed complementary frequencies to those of p.Thr1069Ala (Fig. 2e). This observation suggested that the mosaic UPD was restricted at least to the bone marrow. These results were concordant with the Sanger sequencing results (Figs. S9-10). The degree of mosaicism in the bone marrow tissue changed dynamically over the time course of I-1, but did not strongly correlate with the clinical status of the patient (Fig. S11). These results suggest that compound heterozygous variants that may disable *EFL1* function and impair cell survival formed a cellular environment such that cells with (less damaging) recombinant alleles gained survival advantages over the parental ones (Fig. 2f).

EFL1 deficiency impairs 80S ribosome assembly

Our interpretation of the genetic analysis assumes that the *EFL1* variants are pathogenic, and harbor a gradient of severity (Fig. 2f). More specifically, p.His30Arg possesses a comparable severity with the frameshift variant (p.Gly827TrpfsTer13), and these two are more severe than p.Thr1069Ala. To test this, we measured ribosome assembly function in the presence of

244 the *EFL1* variants, as EFL1 is known to mediate GTP hydrolysis-coupled
245 release of eukaryotic translation initiation factor 6 (eIF6) together with SBDS
246 during the maturation of the 60S ribosome subunit[7,15,16]. Thus, we monitored
247 the ribosomal assembly status of the wild type, siRNA-, or CRISPR/Cas9-
248 mediated ablation of *EFL1* ($EFL1^{KD}$ or $EFL1^{-/-}$) in HeLa and K562 cell lines
249 to further elucidate the molecular function of the mutant protein (Fig. 3a; Fig.
250 S12). Polysome profiling of the $EFL1^{KD}$ and $EFL1^{-/-}$ cells showed a
251 significantly reduced 80S peak (Fig. 3b-c; Fig. S12). This abnormal
252 polysome profile was completely rescued after the introduction of FLAG-
253 tagged wild type *EFL1* but not by the clones that harbored the mutations
254 (Fig. 3b-c; Fig. S13). Interestingly, $EFL1^{p.His30Arg}$ failed to rescue the mutant
255 phenotype, whereas $EFL1^{p.Thr1069Ala}$ displayed a moderate effect on
256 ribosome assembly. These results indicated that EFL1 plays a crucial role in
257 ribosome assembly, and $EFL1^{p.His30Arg}$ possesses a null function, while
258 $EFL1^{p.Thr1069Ala}$ is hypomorphic.
259
260 **Molecular mechanism of EFL1-mediated SDS pathogenesis**
261 Next, we explored the molecular function of the variants in ribosome
262 assembly. Variant function was not mediated via phosphorylation of
263 Thr1069, aberrant subcellular localization of EFL1, or changes in binding
264 affinity to SBDS (Fig. S14). Next, since the release of eIF6 from 60S is a
265 crucial step for 80S assembly and is mediated by SBDS-EFL1, we
266 investigated eIF6 level changes by altering *EFL1*. The assessment of eIF6

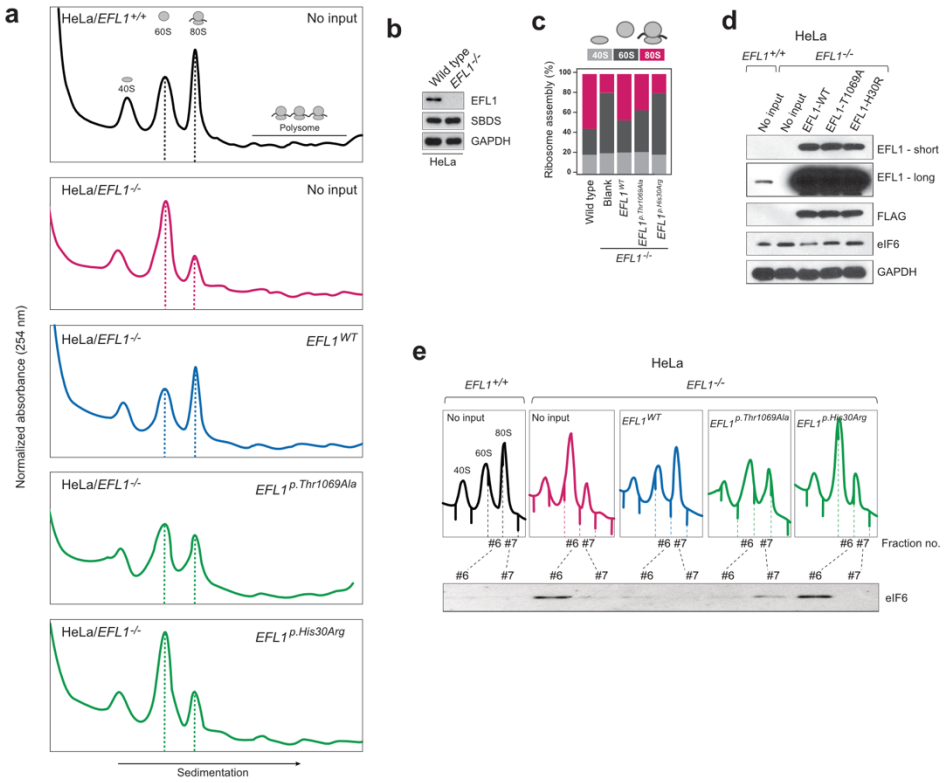

Fig. 3. Nonsynonymous variants in *EFL1* disrupt 80S assembly with varying severities. a Immunoblot showing the CRISPR-knockout of *EFL1* in HeLa cells. **b** Polysome profiling results of *EFL1*$^{+/+}$ and *EFL1*$^{-/-}$ cells followed by transfection of vectors containing *EFL1*^{WT}, *EFL1*$^{p.Thr1069Ala}$ or *EFL1*$^{p.His30Arg}$ (as indicated in the top right corner of each plot). Note the different heights of 60S and 80S peaks in each experiment (dotted lines). **c** Quantification of the polysome profiling results, displaying the relative occupancy of different ribosome statuses. Each bar corresponds to each experiment in (**b**). **d** Immunoblots of EFL1 and eIF6 in wild type or *EFL1*$^{-/-}$ HeLa cells with or without transfection of vectors containing *EFL1*^{WT}, *EFL1*$^{\text{p.Thr1069Ala}}$ or *EFL1*$^{\text{p.His30Arg}}$. **e** Immunoblots of eIF6 from ribosomal fractions that best represent 60S and 80S of HeLa cells, and each corresponds to the polysome profiles shown above.

267

268 in wild type and *EFL1*$^{-/-}$ cells revealed that the absence of *EFL1* induced
269 eIF6 levels, which was partially rescued by the introduction of *EFL1*$^{p.Thr1069Ala}$
270 or *EFL1*$^{p.His30Arg}$ (Fig. 3d). Immunoblot analysis of each ribosomal subunit-
271 bound fraction revealed that eIF6 was more highly enriched in 60S ribosome
272 fraction of the *EFL1*$^{-/-}$ cells as compared to the wild type or *EFL1*-
273 overexpressed cells (Fig. 3e). Remarkably, introduction of *EFL1*$^{p.Thr1069Ala}$
274 rescued the increased eIF6 in the 60S fraction, whereas *EFL1*$^{p.His30Arg}$ failed
275 to do so (Fig. 3e; Fig. S15). Also, absence of *EFL1* caused an impaired
276 shuttling of cytoplasmic eIF6 back to the nucleus, consistent with the
277 previous observation (Fig. S16)[15]. This result, along with the observation
278 that changes in eIF6 and SBDS were not due to transcription levels (Fig.
279 S17), implies that the blocked exclusion of eIF6 and SBDS from the 60S
280 ribosomal subunit is one of the mechanisms by which our mutant protein
281 functions, which results in impaired 80S ribosome assembly. This result also
282 supports our hypothesis that the severity of p.His30Arg is higher than that of
283 p.Thr1069Ala.
284
285 **Deficiency of *EFL1* orthologs reproduces SDS phenotypes in zebrafish**
286 **and mouse models**
287 To determine whether the milder allele (*EFL1*$^{p.Thr1069Ala}$) was still pathogenic
288 enough to cause SDS, a morpholino-targeting zebrafish model of *efl1* was
289 subjected to rescue experiments (Fig. S18). The *efl1* morphants had smaller
290 heads and eyes as wells as slightly bent tails and displayed an increased

291 number of apoptotic cells during development (Fig. 4a). Also, primitive

292 erythrocytes and granulocytes were significantly reduced in the *efl1*

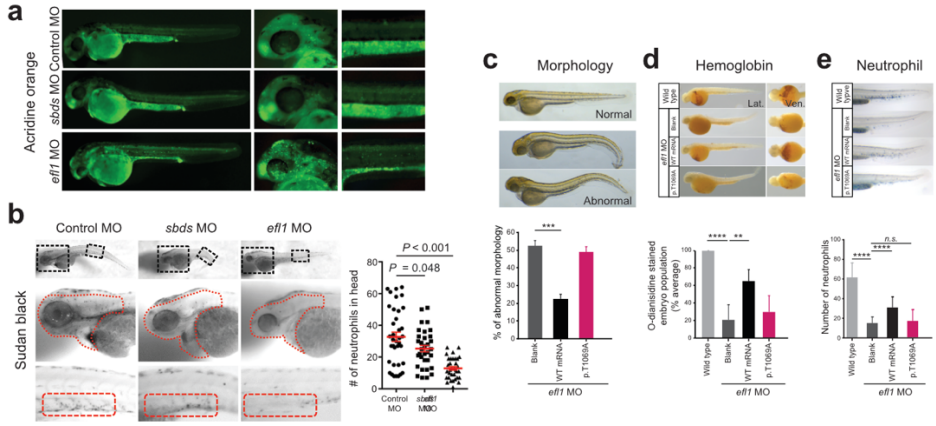

Fig. 4. Zebrafish *efl1* mutants model human SDS features. a-b Cell death (**a**) and neutrophil production (**b**) of 48 hpf zebrafish embryos by the knockdown of *efl1* and *sbds*. (**c-e**) Rescue of *efl1* MO animals using human $EFL1^{WT}$ or $EFL1^{p.Thr1069Ala}$ RNA, documenting morphology (**c**), hemoglobin production (**d**) and neutrophil production (**e**). **, $P < 0.01$; ***, $P < 0.0005$; ****, $P < 0.0001$. hpf, hours post fertilization.

293

294 morphants, indicating impaired primitive hematopoiesis in these embryos

295 (Fig. 4a-b). All phenotypes were rescued by the introduction of the wild type

296 human *EFL1* mRNA, but less so by the $EFL1^{p.Thr1069Ala}$ mRNA (Fig. 4c-e),

297 confirming that the milder *efl1* allele caused SDS-like features in zebrafish.

298 In addition, mouse models were created to further investigate the

299 impact of *Efl1* dysfunction. *Efl1* knock-out and p.Thr1076Ala knock-in mice

300 (mouse Thr1076 is orthologous to human Thr1069; herein designated as

301 $Efl1^{m}$) were generated and subjected to phenotypic analyses (Fig. S19).

302 Embryos that were homozygous for the null allele ($Efl1^{-/-}$) were not retrieved

303 on embryonic day (E) 8.5, implying the essential requirement of the gene in
304 early embryogenesis (Fig. S19). On the other hand, mice homozygous for
305 the knock-in allele (*Efl1*$^{m/m}$) were viable and healthy (Fig. S19), indicating a
306 differential phenotypic tolerance between mice and humans. To model an
307 accurate *Efl1* dose that may induce an SDS-like phenotypic expression, we
308 inter-crossed the two strains and compared phenotypes of the compound
309 heterozygous (CH) animals (*Efl1*$^{m/-}$) to the littermates (*Efl1*$^{+/+}$, *Efl1*$^{+/-}$ and
310 *Efl1*$^{+/m}$), with an emphasis on the major SDS symptoms. The CH mice were
311 smaller (Fig. 5a-b) and died earlier (Fig. 5c). The blood counts revealed
312 reduced hemoglobin, white blood cells and platelets (Fig. 5d), and the bone
313 marrow images displayed a consistent deficiency (Fig. 5e). These results
314 validated our observation that the reduced function of the *EFL1*$^{p.Thr1069Ala}$
315 variant caused SDS in human patients. To determine whether Efl1
316 expression was affected by the *Efl1*^{m} variant, we measured the protein
317 expression from E17.5 livers (Fig. 5f). The liver heterozygous for *Efl1*^{m}
318 (*Efl1*$^{+/m}$) showed reduced Efl1 expression, suggesting that the variant not
319 only reduced Efl1 activity, but also destabilized the protein. The expression
320 of eIF6 was also detected in the CH livers and was increased compared to
321 the wild type livers, which was consistent with our previous observation in
322 the HeLa cells (Fig. 5g). Ribosome profiling of the wild type and CH livers
323 revealed that the CH livers showed a lower 80S peak compared to the wild
324 type livers (Fig. 5h-i).
325

326

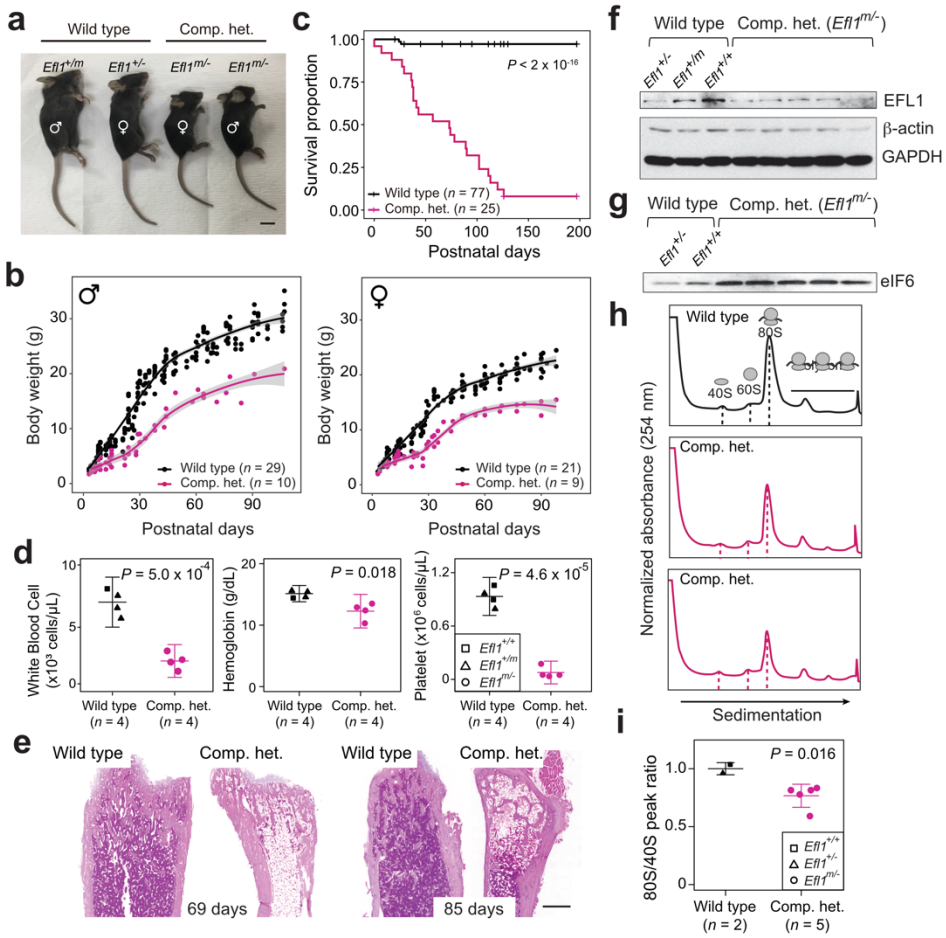

Fig. 5. Mouse *Efl1* mutants model human SDS features. a Body sizes of the CH mice (*Efl1*$^{m/-}$) at three weeks compared to the wild type littermates. **b** Body weight curves of the CH animals compared to the wild types. Males (left) and females (right) are plotted separately. **c** Survival plot. **d** Hematopoietic features of the CH animals, measured at postnatal days 35-42. **e** H&E staining of the bone marrows from 69- and 85-day-old femurs. **f** Level of Efl1 protein in the wild type or CH livers. **g** Immunoblots of eIF6 from wild type or CH livers. **h** Polysome profiling results of the wild type or CH mouse livers. **i** Quantification of the polysome profiling results. Scale bars in (**a**) and (**e**) = 1 cm and 0.5 mm.

329 **Screening downstream factors of EFL1 dysfunction**

330 To further investigate the features of downstream genes that are strongly
331 affected by the reduced EFL1 function, we performed RNA-seq on the total
332 RNA, 40S-, 80S- and polysome-bound RNAs from wild type and *EFL1*$^{-/-}$
333 K562 cells (Fig. 6a; Fig. S20). The 60S-bound RNAs were not analyzed as it
334 is unlikely that the large subunit will bind with RNA by itself. The 248 genes
335 that were decreased in the 80S-bound fraction compared to the 40S-bound
336 fraction in the mutant cells were extracted. A gene ontology analysis
337 suggests that RP genes (GO:0003735) were the major constituents of the
338 genes that were reduced by the absence of *EFL1* (P_{adj} = 5.2 x 10^{-77},
339 adjusted by the Benjamini-Hochberg method; Fig. 6b-c). There was no
340 significantly enriched gene group in the increased gene set. The fractions of
341 the transcripts bound by 40S-, 80S-, or polysome differed substantially for
342 the RP genes in the absence of *EFL1* (P < 1.0 x 10^{-13} for differences in both
343 40S- and 80S-bound transcripts, Wilcoxon signed-rank test), whereas the
344 *TP53* target genes and all other genes did not show such a change (Fig. 6d,
345 P > 0.05, Wilcoxon signed-rank test). Next, we compared whether transcript
346 sizes (Fig. S21), expression levels, or consensus sequence elements in the
347 5' UTRs may serve as a factor that enabled RP-specific regulation. Notably,
348 highly-expressed RP transcripts with a terminal oligo-pyrimidine (TOP)
349 element (5'-CUUYCUUUUNS-3') were specifically altered (Fig. 6e; Fig. S22;
350 P = 6.9 x 10^{-7}). This result revealed that, among all the genes in the

genome, 80S ribosome assembly of RP transcripts containing a TOP element were heavily dependent on the normal EFL1 function.

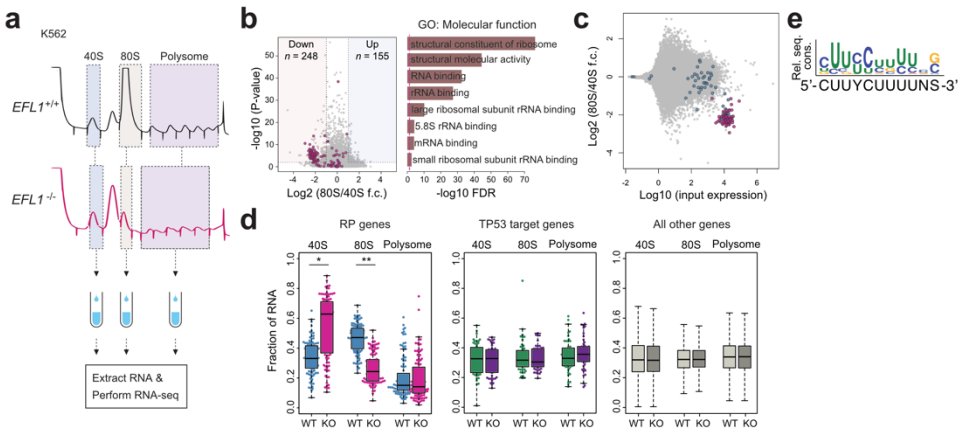

Fig. 6. EFL1 is required for RP synthesis. a Schematic diagram of the RNA expression analysis from K562 ribosomal fractions. **b** Volcano plot of the genes that were differentially enriched in the 80S fraction compared to the 40S fraction (left). GO analysis of the 248 downregulated genes (right). Red dots depict RP genes (GO:0022625 and GO:0022627, n = 118). **c** Fold change of 80S enriched genes normalized by 40S, depicted against transcriptome. Red; significantly downregulated RP genes in (**b**). Blue; other RP genes. **d** Fractions of 40S-, 80S- or polysome-bound RNAs for RP genes (n = 108, left), *TP53* target genes (n = 51, middle) and all other genes (n = 11,812, right) are displayed. Wilcoxon signed-rank test, *. $P = 4.7 \times 10^{-14}$, **. $P = 1.5 \times 10^{-26}$. All other test P-values > 0.05. **e** Consensus sequence profile of downregulated RP gene 5' UTRs, deducing a TOP sequence. Rel. seq. cons. denotes relative sequence conservation from the MEME run.

356 **Discussion**

357

358 We identified and described a unique bone marrow-specific somatic UPD
359 event that preferentially selects cells with *EFL1* alleles of a weaker severity.
360 Although other parts of the body may suffer from biallelic variants in *EFL1*,
361 composed of more damaging one and the milder one, the hematological
362 system was partially rescued by a somatic UPD resulting in a homozygous
363 $EFL1^{p.Thr1069Ala}$ with a weaker severity. We provided evidence suggesting that
364 the majority of the cells that carry $EFL1^{p.Thr1069Ala}$ in a homozygous manner is
365 still pathogenic. We hypothesize that a somatic UPD in the patients could
366 occur and be detected because of the dynamic nature of bone marrow,
367 where the whole stem cell can be potentially replaced by a few clones.
368 Indeed, the somatic UPD was not detected in other solid organs or tissues
369 that were available for investigation. Two lines of evidence suggest
370 infrequent LOH events in the *EFL1* locus in normal populations (2.7-7.7 x
371 10^{-4}; see Results). The odds of having all the p.Thr1069Ala and p.His30Arg
372 variants and the LOH by UPD in the *EFL1* locus for one person by chance is
373 roughly estimated as 1 in 3 trillion, indicating that detectable UPD is not an
374 independent event but is associated with the biallelic *EFL1* variants. It is still
375 not clear if the EFL1 dysfunction somehow contributed to the occurrence of
376 UPD, causing the resulting clone to be expanded by positive selection.
377 Nevertheless, the degree of mosaicism did not seem to directly determine
378 clinical severity (Fig. S11). One could further delineate a more accurate

379 temporal and spatial occurrence of the event if additional clinical samples
380 become available.
381 Several lines of evidence from our experiments suggest that
382 although p.Thr1069Ala is the mildest among the variants that we found, it is
383 still functional and hypomorphic: (1) the parents of patients that were
384 heterozygous for *EFL1*$^{p.Thr1069Ala}$ were asymptomatic, whereas the patients
385 carried the variant in a homozygous status in their bone marrow and
386 showed the pathology; (2) a ribosome profiling assay using a variant allele
387 partially rescued the 80S assembly problem, whereas the wild type allele
388 completely rescued it (Fig. 3); (3) *efl1* MO-treated zebrafish were partially
389 rescued by the variant-containing RNA (Fig. 4); and (4) *Efl1*$^{m/-}$ mice
390 displayed an SDS-like phenotype, which was of an intermediate severity
391 relative to the *Efl1*$^{-/-}$ and *Efl1*$^{+/-}$ mice (Fig. 5). It is notable that although our
392 mouse model successfully phenocopied most of the SDS features, the
393 genotype was not in complete concordance with that of human patients. Our
394 mouse model with *Efl1*$^{m/m}$ did not show significant phenotypes, whereas
395 human patients with bone marrow specific homozygous *EFL1*$^{p.Thr1069Ala}$ by
396 somatic UPD still had hematological abnormalities such as anemia and
397 neutropenia. This discrepancy between the two species is not rare[23,24], and
398 it again underscores differences in tolerance to a given variant, perhaps due
399 to different physiological and genetic systems, which is critical in modeling
400 human clinical features in mice.

401 Nonetheless, we demonstrated that the altered function of EFL1
402 specifically influenced the translation of RP genes containing a TOP element
403 in the 5' UTR, which led to a mechanistic mimicry of Diamond-Blackfan
404 anemia, which is another ribosomopathy caused by insufficient RP
405 doses[25,26]. The activation of TP53 is considered as a targetable downstream
406 pathway that leads to SDS or a DBA phenotype[27-29]. However, our data
407 suggest that the loss of *EFL1* does not induce TP53 activation, which is
408 consistent with previous studies of the zebrafish *sbds* model and DBA (Fig.
409 6d)[30,31].
410 It is known that LARP1 directly binds to the TOP element of RP
411 genes to repress translation in a phosphorylation-dependent manner and
412 that mTOR partially regulates LARP1 phosphorylation[32,33]. To determine if
413 we could utilize this pathway to de-repress RP translation and rescue the
414 SDS phenotype in the animal models, we considered a molecular signaling
415 pathway that may regulate RP gene translation through the TOP element.
416 However, both LARP1 binding to RP TOP elements and mTOR signaling
417 were unchanged in the mutant cells, suggesting an alternative mechanism
418 that may regulate RP translation (data not shown).
419 Here, we demonstrated a mechanism by which biallelic variants of
420 *EFL1* phenocopied classical SDS in three unrelated patients. The bone
421 marrow-specific somatic UPD in these patients mitigated the potentially
422 catastrophic hematological phenotype by homozygosing the less damaging
423 variant (*EFL1*$^{p.Thr1069Ala}$). We demonstrated that defective EFL1 caused

424 impaired 80S ribosomal assembly and that the zebrafish and mouse models
425 displayed similar features to humans through the alteration of 80S ribosome
426 assembly of RP transcripts. An extensive search of such SDS patients may
427 provide more insight into the development of somatic mosaicism and
428 subsequent molecular cascades that may lead to new avenues of treatment
429 for ribosomopathy.
430

431 **Materials and methods**

432

433 *Patient recruitment and sampling*

434 Patient enrollment and sampling were conducted under the approval of the
435 Institutional Review Board of Seoul National University Hospital (IRB number:
436 H-1408-014-599). Patients or their parents were provided an informed
437 consent for genetic testing and collecting blood, buccal swab, scalp hair, urine
438 and clipped nails. Biopsy samples of I-1 (esophagus, stomach, duodenum,
439 colon and liver) were retrieved from the Department of Pathology of Seoul
440 National University for a research purpose.

441

442 *Whole exome sequencing and variant calling*

443 Trio whole exome sequencing (WES) was performed on one family (I-1, I-2,
444 and I-3) and singleton WES for two families (II-1 and III-1) at Theragen Etex
445 (Suwon, Korea) using genomic DNA extracted from whole blood. Exome was
446 captured using SeqCap EZ Exome v2 Kit (Roche Sequencing, Madison, WI)
447 or SureSelect Human All Exon V5 (Agilent Technologies, Santa Clara, CA)
448 and sequenced by HiSeq 2500 or HiSeq 4000 (Illumina, Inc., San Diego, CA).
449 Paired-end sequencing was performed with read lengths of 75 or 100 base
450 pairs. The raw reads were aligned by BWA MEM software [34]. Variants were
451 called by Samtools and annotated by in-house pipeline and SnpEff [34-36].

452

453 *Single nucleus SNP microarray*

454 Nuclei of frozen bone marrow cells from I-1, where a majority of the cells were
455 disrupted during freezing, were prepared and collected manually with a
456 pipette under a phase-contrast microscope. Buccal swab of III-1 was
457 resuspended in 1 ml of PBS and centrifuged at 300 *g* for 3 min. Supernatant
458 was discarded and pellet was resuspended in PBS. This suspension was
459 moved to a 100 ml cell culture dish. Single cells were manually picked up with
460 a pipette under a phase-contrast microscope. These single cells or nuclei
461 were whole-genome amplified by a REPLI-g Single Cell Kit (Qiagen, Venlo,
462 the Netherlands) for 3 hours. Amplified genomes were genotyped by Infinium®
463 OmniExpress-24 v1.2 (Illumina, Inc.).
464
465 *Sample-barcoded amplicon sequencing*
466 Genomic DNAs extracted from multiple individuals and tissues were PCR
467 amplified with primers shown in Table S6, with following condition: 3 min at
468 95°C, followed by 20 cycles (30 sec at 95°C, 30 sec at 57°C, and 20 sec at
469 72°C), and a final extension at 5 min at 72°C. Barcoded PCRs were
470 performed with 1 μl of first PCR product as templates using tissue-specific
471 barcoded primers (Table S7). Same reverse, forward and reverse primers of
472 *EFL1*, *WDR76* and rs1044032 with Sanger sequencing were used for
473 barcoded PCR products, respectively. The second PCR condition was: 3 min
474 at 95°C, followed by 20 cycles (30 sec at 95°C, 30 sec at 57°C, and 20 sec
475 at 72°C), and a final extension at 5 min at 72°C.
476

Molecular dynamics (MD) simulation of EFL1

The initial atom coordinates for MD simulations were from the Protein Data Bank accession number 5ANC [7]. Input files were prepared with PSFGEN, SOLVATE, and IONIZE plug-ins of VMD [37]. Each simulation used explicit TIP3 solvent and periodic boundaries. Each unit cell contained one molecule of the entire preinitiation complex. The unit cells were ~210 Å x 180 Å x 190 Å in size and contained ~700,000 atoms. Sodium and chloride were added to make the total ionic strength 100 mM. MD simulations were performed in triplicate (each 50 ns in length) with a CHARMM36 force field [38] using NAMD2 [39] on the Bebop cluster of the Laboratory Computing Resource Center at Argonne National Laboratory. MD simulations were run at P = 1 atm, T = 310 K, with a 1 fs integration time and a 12 Å cutoff distance. Nonbonded forces were calculated every two steps and electrostatic forces were calculated every four. Pressure and temperature were maintained using a Langevin piston and bath. Atom coordinates were recorded every 10 ps. MD trajectories were visualized and analyzed with VMD and PyMol.

Polysome profiling

To maintain the binding of mRNA to ribosome subunits, cycloheximide (Sigma-Aldrich, St. Louis, MO) (100 ug/ml) was added to cell culture media and incubated for 10 min at 37°C. After incubation, cells were washed with cold PBS including cycloheximide (10 ug/ml) twice, then lysed with 1 ml of polysome lysis buffer (20 mM HEPES pH 7.6, 5 mM $MgCl_2$, 125 mM KCl, 1%

500 NP-40, 2 mM DTT) supplemented with cycloheximide (100 ug/ml), protease
501 inhibitor cocktail (EDTA-free; Roche) and RNase inhibitor (Invitrogen,
502 Carlsbad, CA) on ice. Cell lysates were tumbled for 20 min at 4°C and
503 centrifuged at 13,200 rpm for 20 min. The supernatants were fractionated in
504 17.5-50% linear sucrose gradients by ultracentrifugation (35,000 rpm for 160
505 min) in a Beckman ultracentrifuge using SW41-Ti rotor. Gradients were eluted
506 with a gradient fractionator (Brandel, Gaithersburg, MD) and monitored with
507 a UA-5 detector (ISCO). Equal volume of each polysome fraction was used
508 for determining the level of eIF6 by Western blot analysis.
509
510 RNA sequencing from polysome fractions
511 RNA was extracted from polysome fractionation. RNA sequencing library was
512 constructed using a TruSeq stranded total RNA kit (Illumina Inc.) with rRNA
513 depletion. 100 bp paired-end sequencing was performed using HiSeq 2500,
514 producing >5 Gb for each sample. Transcripts with polysome-bound RNA
515 count >10 were selected and subjected to calculation of fractions of 40S-,
516 80S- or polysome-bound RNA molecules for a given gene.
517
518 *Zebrafish experiments*
519 Zebrafish embryos were co-injected with *efl1* morpholino (MO) and normal or
520 mutated human *EFL1* mRNA at 1-2 cell stage. To evaluate the rescue efficacy
521 of each co-injected *EFL1* mRNA, the number of neutrophils and primary
522 erythrocytes were assessed. For neutrophils, individual Sudan Black stained

523 cells in the caudal region of the embryo, posterior to the anal opening, were
524 counted and the absolute number of positive cells were used for phenotypic
525 comparison. For primary erythrocytes, the degree of o-dianisidine staining
526 was qualitatively compared using the percentage of o-dianisidine stained
527 embryos within the population, since it is not technically possible to count
528 individual erythrocytes.
529
530 *Efl1 mutant mouse strain construction, maintenance and experiments*
531 All the mouse experiments were performed under the standard protocols
532 approved by IACUC (#17-0148-S1A0). *Efl1* knock-out (*Efl1*$^{-}$) strain was
533 constructed by introducing a 10-base deletion in the 10th exon of the gene in
534 C57BL6/J strain using CRISPR/Cas9 system in Macrogen (Seoul, Korea).
535 One cell embryos were microinjected with two sgRNAs (5'-
536 ACTTCTTTAGGATTAAAAATTGG-3' and 5'-
537 CCGAGGACAGCGTGGGATATGGG-3') and Cas9 protein mixture,
538 incubated and transplanted into pseudopregnant recipient ICR mice. *Efl1*
539 knock-in (*Efl1*$^{p.Thr1076Ala}$) variant was generated in C57BL6/J in University of
540 Utah Mutation Generation and Analysis Core using two sgRNAs (5'-
541 GTTCTGGGTGCCGACCACGG-3' and 5'-GTGCAGGTACTCCTCCTCCG-
542 3') and in the presence of oligodeoxynucleotides which includes the
543 ACC>GCC change mimicking the p.Thr1069Ala and an *Mbo*I site for
544 genotyping. Genotyping strategies of the wild type and mutant alleles are
545 described in supplemental Methods. For phenotypic evaluations, wild type

546 and mutant mice from the same litter were sacrificed and dissected for
547 peripheral blood extraction, pancreas pathology and skeletal structure
548 analysis. 300 ul of peripheral blood was extracted from 35-42-day animals
549 and subjected to a complete blood count and differential tests.
550

Author contributions

M. Choi, H.J. Kang, and H.H. Kim conceived the study. S. Lee and M. Choi performed genetic analysis and statistical evaluations. C.H. Shin, S. Lee, S.D. Jeong, H.H. Kim, J. Lee, and M. Choi performed molecular biology and biochemistry experiments and assessed the results. J. Lee, S. Lee, S.J. Son, M. Choi, and J.K. Seong performed mouse experiments. J.-D. Kim, A.-R. Kim, and S.-W. Jin performed zebrafish experiments. C.R. Hong, J.S. Ko, Y.B. Sohn, O.-H. Kim, J.M. Ko, T.-J. Cho, and H.J. Kang provided patient care and generated clinical data. N.T. Wright, O. Kokhan, and T. Yoo analyzed protein structure. M. Choi, S. Lee, C.H. Shin, C.R. Hong, J. Lee, H.J. Kang, and H.H. Kim wrote the manuscript. All authors approved the final version of the manuscript.

Acknowledgements

We appreciate the patients and families that participated in this study. We thank Jung-Ah Kim and Hyoung-Jin Kim at Seoul National University Hospital for collecting and interpreting hematological data and for interpreting images. We thank the University of Utah Mutation Generation and Detection Core for construction of the *Efl1* knock-in mice. This study was partly supported by grants from the National Research Foundation of Korea (2014M3C9A2064686, 2019R1A2C2010789 to M.C. and 2017R1A2A2A05069691 to H.H.K.) and National Science Foundation (REU CHE-1062629 and RUI MCB-1607024) awards to N.T.W.. This research

was partly supported by Korea Mouse Phenotyping Project (2013M3A9D5072550) of the Ministry of Science, ICT and Future Planning through the National Research Foundation. OK gratefully acknowledges the computing resources provided by Bebop, a high-performance computing cluster operated by the Laboratory Computing Resource Center at Argonne National Laboratory. The authors declare no competing financial interests.

Abbreviations used: CH, compound heterozygous; DBA, Diamond-Blackfan anemia; LOH, loss of heterozygosity; RP, ribosomal protein; SDS, Shwachman-Diamond syndrome; TOP, terminal oligo-pyrimidine; UPD, uniparental disomy; VUS, variants of unknown significances.

586 **Table 1. Coverage depths and allele frequencies of *EFL1* variants**

Patient	Variant in *EFL1* (M: maternal origin, P: paternal, or U: unknown)	Method	Allele coverage depths (ref. allele:non-ref. allele) (% non-ref. allele)			AF in gnomAD	
			Patient	Mother	Father	Overall	East Asian
I-1	p.Thr1069Ala (M)	WES	10:64 (86.5%)	39:40 (50.1%)	33:0 (0%)	3.2×10^{-5}	1.7×10^{-4}
		Amplicon seq.	23,914:131,714 (84.6%)	63,582:63,954 (50.1%)	121,502:507 (0.4%)		
	p.Gly827TrpfsTer13 (P)	WES	22:2 (8.3%)	27:0 (0%)	9:14 (60.9%)	0	0
		Amplicon seq.	243,610:43,042 (15.0%)	505,158:74 (0.01%)	221,532:218,976 (49.7%)		
II-1	p.Thr1069Ala (U)	WES	15:59 (79.7%)	N/A	N/A	3.2×10^{-5}	1.7×10^{-4}
	p.His30Arg (U)	WES	127:22 (14.8%)	N/A	N/A	1.8×10^{-5}	5.1×10^{-5}
III-1	p.Thr1069Ala (P)	WES	43:30 (41.1%)	N/A	N/A	3.2×10^{-5}	1.7×10^{-4}
		Amplicon seq.	135,196:149,160 (52.5%)	189,517:1,786 (0.9%)	87,347:85,317 (49.4%)		
	p.His30Arg (M)	WES	74:43 (36.8%)	N/A	N/A	1.8×10^{-5}	5.1×10^{-5}
		Amplicon seq.	25,316:22,680 (47.3%)	119,382:121,508 (50.4%)	41,684:76 (0.2%)		

587

References

1 Boocock, G. R. *et al.* Mutations in SBDS are associated with Shwachman-Diamond syndrome. *Nat Genet* **33**, 97-101, doi:10.1038/ng1062 (2003).

2 Shimamura, A. Shwachman-Diamond syndrome. *Semin Hematol* **43**, 178-188, doi:10.1053/j.seminhematol.2006.04.006 (2006).

3 Dror, Y. *et al.* Draft consensus guidelines for diagnosis and treatment of Shwachman-Diamond syndrome. *Ann N Y Acad Sci* **1242**, 40-55, doi:10.1111/j.1749-6632.2011.06349.x (2011).

4 Kuijpers, T. W. *et al.* Hematologic abnormalities in Shwachman Diamond syndrome: lack of genotype-phenotype relationship. *Blood* **106**, 356-361, doi:10.1182/blood-2004-11-4371 (2005).

5 Dror, Y. & Freedman, M. H. Shwachman-Diamond syndrome: An inherited preleukemic bone marrow failure disorder with aberrant hematopoietic progenitors and faulty marrow microenvironment. *Blood* **94**, 3048-3054 (1999).

6 Hashmi, S. K. *et al.* Comparative analysis of Shwachman-Diamond syndrome to other inherited bone marrow failure syndromes and genotype-phenotype correlation. *Clin Genet* **79**, 448-458, doi:10.1111/j.1399-0004.2010.01468.x (2011).

7 Weis, F. *et al.* Mechanism of eIF6 release from the nascent 60S ribosomal subunit. *Nat Struct Mol Biol* **22**, 914-919, doi:10.1038/nsmb.3112 (2015).

8 Menne, T. F. *et al.* The Shwachman-Bodian-Diamond syndrome protein mediates translational activation of ribosomes in yeast. *Nat Genet* **39**, 486-495, doi:10.1038/ng1994 (2007).

9 Narla, A. & Ebert, B. L. Ribosomopathies: human disorders of ribosome dysfunction. *Blood* **115**, 3196-3205, doi:10.1182/blood-2009-10-178129 (2010).

10 Tan, Q. K. *et al.* Further evidence for the involvement of EFL1 in a Shwachman-Diamond-like syndrome and expansion of the phenotypic features. *Cold Spring Harb Mol Case Stud* **4**, doi:10.1101/mcs.a003046 (2018).

11 Stepensky, P. *et al.* Mutations in EFL1, an SBDS partner, are associated with infantile pancytopenia, exocrine pancreatic insufficiency and skeletal anomalies in aShwachman-Diamond like syndrome. *J Med Genet* **54**, 558-566, doi:10.1136/jmedgenet-2016-104366 (2017).

12 Tummala, H. *et al.* DNAJC21 Mutations Link a Cancer-Prone Bone Marrow Failure Syndrome to Corruption in 60S Ribosome Subunit Maturation. *Am J Hum Genet* **99**, 115-124, doi:10.1016/j.ajhg.2016.05.002 (2016).

13 Dhanraj, S. *et al.* Biallelic mutations in DNAJC21 cause Shwachman-Diamond syndrome. *Blood* **129**, 1557-1562, doi:10.1182/blood-2016-08-735431 (2017).

14 Carapito, R. *et al.* Mutations in signal recognition particle SRP54 cause syndromic neutropenia with Shwachman-Diamond-like features. *J Clin Invest* **127**, 4090-4103, doi:10.1172/JCI92876 (2017).
15 Tan, S. *et al.* EFL1 mutations impair eIF6 release to cause Shwachman-Diamond syndrome. *Blood* **134**, 277-290, doi:10.1182/blood.2018893404 (2019).
16 Finch, A. J. *et al.* Uncoupling of GTP hydrolysis from eIF6 release on the ribosome causes Shwachman-Diamond syndrome. *Genes Dev* **25**, 917-929, doi:10.1101/gad.623011 (2011).
17 Chase, A. *et al.* PRR14L mutations are associated with chromosome 22 acquired uniparental disomy, age-related clonal hematopoiesis and myeloid neoplasia. *Leukemia* **33**, 1184-1194, doi:10.1038/s41375-018-0340-5 (2019).
18 Dubois, V. *et al.* Pretransplant HLA mistyping in diagnostic samples of acute myeloid leukemia patients due to acquired uniparental disomy. *Leukemia* **26**, 2079-2085, doi:10.1038/leu.2012.68 (2012).
19 Roberts, J. L. *et al.* CD45-deficient severe combined immunodeficiency caused by uniparental disomy. *Proc Natl Acad Sci U S A* **109**, 10456-10461, doi:10.1073/pnas.1202249109 (2012).
20 Swensen, J. J. *et al.* Sickle cell disease resulting from uniparental disomy in a child who inherited sickle cell trait. *Blood* **116**, 2822-2825, doi:10.1182/blood-2010-05-284331 (2010).
21 Lek, M. *et al.* Analysis of protein-coding genetic variation in 60,706 humans. *Nature* **536**, 285-291, doi:10.1038/nature19057 (2016).
22 Loh, P. R. *et al.* Insights into clonal haematopoiesis from 8,342 mosaic chromosomal alterations. *Nature* **559**, 350-355, doi:10.1038/s41586-018-0321-x (2018).
23 el-Amraoui, A. *et al.* Human Usher 1B/mouse shaker-1: the retinal phenotype discrepancy explained by the presence/absence of myosin VIIA in the photoreceptor cells. *Hum Mol Genet* **5**, 1171-1178, doi:10.1093/hmg/5.8.1171 (1996).
24 Liao, B. Y. & Zhang, J. Null mutations in human and mouse orthologs frequently result in different phenotypes. *Proc Natl Acad Sci U S A* **105**, 6987-6992, doi:10.1073/pnas.0800387105 (2008).
25 Draptchinskaia, N. *et al.* The gene encoding ribosomal protein S19 is mutated in Diamond-Blackfan anaemia. *Nat Genet* **21**, 169-175, doi:10.1038/5951 (1999).
26 Khajuria, R. K. *et al.* Ribosome Levels Selectively Regulate Translation and Lineage Commitment in Human Hematopoiesis. *Cell* **173**, 90-103 e119, doi:10.1016/j.cell.2018.02.036 (2018).
27 Danilova, N., Sakamoto, K. M. & Lin, S. Ribosomal protein S19 deficiency in zebrafish leads to developmental abnormalities and defective erythropoiesis through activation of p53 protein family. *Blood* **112**, 5228-5237, doi:10.1182/blood-2008-01-132290 (2008).
28 McGowan, K. A. *et al.* Ribosomal mutations cause p53-mediated dark skin and pleiotropic effects. *Nat Genet* **40**, 963-970,

doi:10.1038/ng.188 (2008).

29 Elghetany, M. T. & Alter, B. P. p53 protein overexpression in bone marrow biopsies of patients with Shwachman-Diamond syndrome has a prevalence similar to that of patients with refractory anemia. *Arch Pathol Lab Med* **126**, 452-455, doi:10.1043/0003-9985(2002)126<0452:PPOIBM>2.0.CO;2 (2002).

30 Provost, E. *et al.* Ribosomal biogenesis genes play an essential and p53-independent role in zebrafish pancreas development. *Development* **139**, 3232-3241, doi:10.1242/dev.077107 (2012).

31 Ludwig, L. S. *et al.* Altered translation of GATA1 in Diamond-Blackfan anemia. *Nat Med* **20**, 748-753, doi:10.1038/nm.3557 (2014).

32 Tcherkezian, J. *et al.* Proteomic analysis of cap-dependent translation identifies LARP1 as a key regulator of 5'TOP mRNA translation. *Genes Dev* **28**, 357-371, doi:10.1101/gad.231407.113 (2014).

33 Fonseca, B. D. *et al.* La-related Protein 1 (LARP1) Represses Terminal Oligopyrimidine (TOP) mRNA Translation Downstream of mTOR Complex 1 (mTORC1). *J Biol Chem* **290**, 15996-16020, doi:10.1074/jbc.M114.621730 (2015).

34 Li, H. & Durbin, R. Fast and accurate long-read alignment with Burrows-Wheeler transform. *Bioinformatics* **26**, 589-595, doi:10.1093/bioinformatics/btp698 (2010).

35 Li, H. *et al.* The Sequence Alignment/Map format and SAMtools. *Bioinformatics* **25**, 2078-2079, doi:10.1093/bioinformatics/btp352 (2009).

36 Cingolani, P. *et al.* A program for annotating and predicting the effects of single nucleotide polymorphisms, SnpEff: SNPs in the genome of Drosophila melanogaster strain w1118; iso-2; iso-3. *Fly (Austin)* **6**, 80-92, doi:10.4161/fly.19695 (2012).

37 Humphrey, W., Dalke, A. & Schulten, K. VMD: visual molecular dynamics. *J Mol Graph* **14**, 33-38, 27-38, doi:10.1016/0263-7855(96)00018-5 (1996).

38 Best, R. B. *et al.* Optimization of the additive CHARMM all-atom protein force field targeting improved sampling of the backbone phi, psi and side-chain chi(1) and chi(2) dihedral angles. *J Chem Theory Comput* **8**, 3257-3273, doi:10.1021/ct300400x (2012).

39 Phillips, J. C. *et al.* Scalable molecular dynamics with NAMD. *J Comput Chem* **26**, 1781-1802, doi:10.1002/jcc.20289 (2005).